Gradient-index phononic crystals

Sz-Chin Steven Lin and Tony Jun Huang*
Department of Engineering Science and Mechanics, The Pennsylvania State University, University Park, Pennsylvania 16802, USA

Jia-Hong Sun and Tsung-Tsong Wu
Institute of Applied Mechanics, National Taiwan University, Taipei 106, Taiwan

(Received 30 October 2008; revised manuscript received 13 January 2009; published 18 March 2009)

We designed and characterized a two-dimensional, gradient-index phononic crystal (GRIN PC) to control the propagation of acoustic waves. The GRIN PC was composed of solid cylinders arranged in a square lattice and immersed in an epoxy. The refractive index along the direction transverse to the phononic propagation was designated as a hyperbolic secant gradient distribution. This distribution was modulated by means of the density and elastic moduli of the cylinders. The effective refractive indices in each row of the GRIN PC were determined from band diagrams obtained via a plane-wave expansion method. The acoustic wave propagation was numerically investigated by a finite-difference time-domain method, and the results were compared to the analytical beam trajectories derived from the hyperbolic secant profile. These results show that the GRIN PC allows acoustic focusing over a wide range of working frequencies, making it suitable for applications such as flat acoustic lenses and couplers.

DOI: 10.1103/PhysRevB.79.094302 PACS number(s): 63.20.−e, 43.20.+g, 46.40.Cd

I. INTRODUCTION

Phononic crystals (PCs) are periodic structures that are engineered to manipulate the propagation of acoustic waves.[1,2] For wavelengths on the scale of the structures' periodicity, PCs exhibit phononic band gaps, frequency ranges where acoustic waves cannot propagate. The phononic band gaps of unbounded PCs, semi-infinite PCs, and PC plates have been investigated,[3–11] and such PCs have been employed as waveguides[12–15] and couplers.[16] It has recently been theoretically and experimentally shown that flat PCs exhibit negative refraction within partial phononic band gaps, where PCs are highly anisotropic.[17–20] This discovery has paved the way for PC-based acoustic lenses. Traditional acoustic lenses with curved surfaces are difficult to fabricate and are prone to misalignment. Thus, PC-based flat lenses may prove advantageous in many applications, especially in micro/nanoscale systems where one cannot readily fabricate small-scale convex or concave lenses.

Despite the promise of PC-based flat lenses, negative refraction in PCs has previously been observed only within narrow frequency bands and for certain incident angles. As such, PC lenses that focus acoustic waves by means of negative refraction feature restricted ranges of operation, large focal zones, and low gain.[17] Moreover, existing PC lenses operate within the first partial band gap or within higher-order dispersion bands. In both cases, the reduced frequency ($\Omega = fa/C$, where f is the working frequency, a is the lattice spacing of the structure, and C is the sound velocity in background material) is high. Since the reduced frequency is proportional to lattice spacing, a PC lens designed at a high reduced frequency may be more convenient to fabricate, but it is too bulky to be integrated with the existing acoustic systems that are used in applications such as biomedical imaging, cell sonoporation, and nondestructive evaluation (NDE).

The aforementioned limitations call for the development of a flat acoustic lens that operates over wide ranges at low reduced frequencies. Hakansson *et al.*[21] recently presented a design of PC lenses via inverse design method that meets the requirement of larger bandwidth. In this work, we demonstrate a wide-band flat PC lens by means of two-dimensional (2D), gradient-index phononic crystals (GRIN PCs). Our lens was inspired from gradient-index optics, where bending, converging, and collimation of light have been demonstrated.[22–26] We found computationally that a 2D GRIN PC lens, an analog of the GRIN optical lens, allowed effective acoustic focusing over a wide band. The design of the GRIN PC is detailed in Sec. II. We introduced an analytic expression to describe the beam trajectory within a GRIN medium and calculated the effective refractive indices in each row of the GRIN PC for the shear vertical (SV) mode bulk acoustic wave (BAW) by a plane-wave expansion (PWE) method. In addition, we simulated SV-mode bulk acoustic wave propagation within the GRIN PC by a finite-difference time-domain (FDTD) method. The simulation results and discussion are presented in Sec. III. Lastly, we studied how the focal length of the GRIN PC related to operating frequency.

II. DESIGN OF THE GRADIENT-INDEX PHONONIC CRYSTAL

Our goal when designing a GRIN structure was to select a refractive index profile that enables acoustic wave focusing. The simplest profile is of parabolic form, and it is widely studied and used in optical devices. We chose a refractive index profile in the form of a hyperbolic secant (of which a parabolic profile can be considered as the first-order Taylor series approximation).[25] One can analytically solve the equations that govern wave propagation within the hyperbolic secant gradient media; this solution is not an approximation, causing minimum aberration. The refractive index profile of a 2D, continuous GRIN medium along the transverse direction (y axis) was defined as

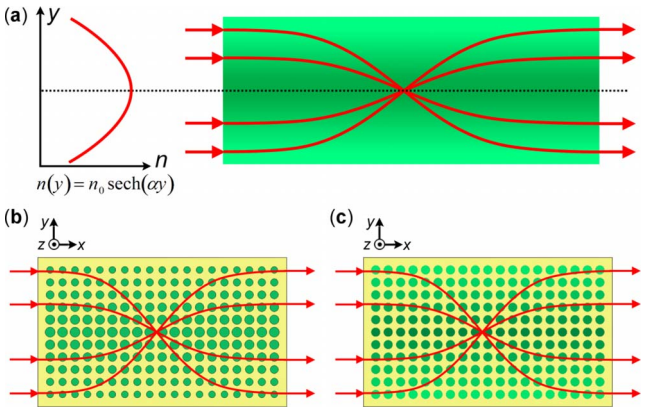

FIG. 1. (Color online) (a) Principle of a gradient-index medium. A hyperbolic secant refractive index profile along the direction transverse to propagation (y axis) enables redirection of incident beams (arrows) inside the medium. A GRIN PC can be realized by (b) adjusting radii of cylinders or (c) changing elastic properties of cylinders along the transverse direction to achieve a hyperbolic secant refractive index profile.

$$n(y) = n_0 \operatorname{sech}(\alpha y), \tag{1}$$

where n_0 is the refractive index along the center axis (x axis) and α is the gradient coefficient. Within the GRIN medium, the paraxial incident beams bent gradually toward the center axis where refractive index was highest (per Snell's law) and converged at a focal spot. Beyond that spot, the focused beams were redirected parallel to the direction of propagation, as shown in Fig. 1(a). A flat GRIN medium can thereby serve as a flat lens for focusing or for collimation. The beam trajectory within a GRIN medium can be analytically derived from the hyperbolic secant refractive index profile:[22]

$$y(x) = \frac{1}{\alpha}\sinh^{-1}[u_0 H_f(x) + \dot{u}_0 H_a(x)], \tag{2}$$

where u_0 is the hyperbolic space at $x=0$ such that $u_0 = \sinh(\alpha y_0)$; $\dot{u}_0$ is the derivative of u_0 with respect to x; and $H_a(x)$ and $H_f(x)$ are the positions of axial and field rays written as

$$H_a(x) = \sin(\alpha x)/\alpha, \quad H_f(x) = \cos(\alpha x). \tag{3}$$

The sinusoidal path through the GRIN medium described by Eq. (2) features a focal length (the distance to focus paraxial incident beams within the GRIN medium) of

$$f = \pi/2\alpha. \tag{4}$$

The focal length is independent of the incident position along the y direction (y_0). One may thus characterize focusing within a GRIN medium by the gradient coefficient α.

A 2D GRIN PC can be considered as a transversely discretized medium where each row is independently homogeneous and isotropic. One can physically realize this discretized medium by adjusting the refractive index in each row to fit a hyperbolic secant profile. The adjustments may be realized by changing the radiuses or elastic properties of the cylinders in each row, as illustrated in Figs. 1(b) and 1(c), respectively. Though PCs are anisotropic and frequency dispersive, the effective refractive index for a certain wave mode of a PC that is driven at a specific frequency can be approximated as the average of the refractive indices along its principal orientations.[23,27] For small anisotropic ratios where equal-frequency contours (EFCs) are nearly circular, the effective refractive index for the considered wave mode of a square-lattice PC is given by

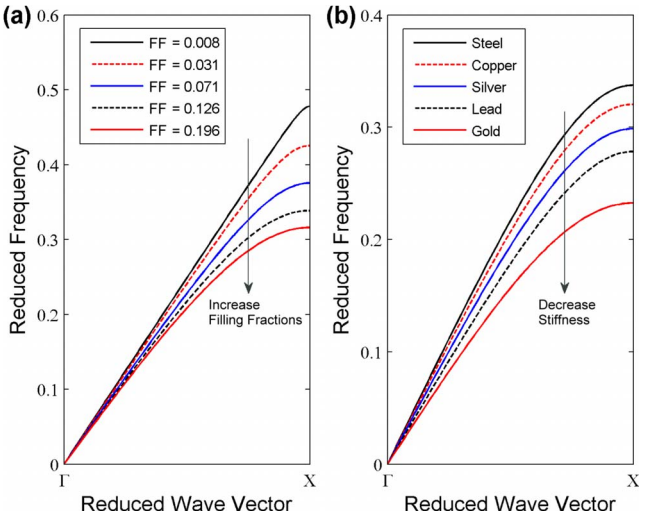

FIG. 2. (Color online) Band diagrams of the first SV bulk acoustic mode along the ΓX orientation (a) for various filling fractions (FFs) of a steel/epoxy PC, and (b) for PCs consist of different solid cylinders in epoxy with a filling fraction of 0.126. The frequency is reduced by a factor of a/C, where a is the lattice spacing of the structure and C is the transverse velocity within the epoxy. The group velocity of a PC decreases when the filling fraction increases or the cylinder stiffness decreases.

$$n_{\text{eff}} = \frac{n_{\Gamma X} + n_{\Gamma M}}{2}. \tag{5}$$

Here $n_{\Gamma X}$ and $n_{\Gamma M}$ are refractive indices along the ΓX and ΓM orientations, respectively:

$$n_{\Gamma X} = \frac{C}{v_{\Gamma X}} = \frac{C}{d\omega/dk_{\Gamma X}}, \quad n_{\Gamma M} = \frac{C}{v_{\Gamma M}} = \frac{C}{d\omega/dk_{\Gamma M}}, \tag{6}$$

where v is the group velocity of the considered wave mode and C is the sound velocity of the propagation mode in background material. We calculated the band diagrams of PCs by a PWE method[2,3] to determine the refractive indices, and we only considered the shear vertical bulk acoustic wave mode of displacement polarized along the z axis. We plotted the band diagrams of the first SV mode along the ΓX orientation for various filling fractions of a steel/epoxy PC [Fig. 2(a)], as well as for PCs of different solid cylinders in epoxy with a filling fraction of 0.126 [Fig. 2(b)]. The SV group velocity of a PC decreased (and the refractive index increased) when the filling fraction was increased or the cylinder stiffness was decreased. A 2D GRIN PC can thus be formed by carefully adjusting cylinder radii or choosing appropriate materials in different rows to match a hyperbolic secant refractive index profile.

TABLE I. Elastic properties of the materials used in the GRIN PC. The effective refractive indices were obtained at reduced frequency $\Omega=0.10$ with a PWE method, per Eq. (5).

Material	y coordinate	Density (g/cm^3)	V_l (km/s)	V_s (km/s)	$N_{\text{eff}}(\Omega=0.10)$
Cadmium	0	8.6	2.8	1.5	1.186
Molybdenum	±1	10.1	6.29	3.35	1.184
Titanium carbide	±2	10.15	6.7	4.0	1.178
Copper	±3	8.96	4.66	2.24	1.168
Niobium	±4	8.57	4.92	2.1	1.160
Brass	±5	8.1	4.7	2.1	1.144
Cast iron	±6	7.7	5.9	2.4	1.123
Zinc	±7	7.1	4.2	2.41	1.102
Chromium	±8	7.0	6.65	4.03	1.073
Zinc oxide	±9	5.68	6.33	2.95	1.042
Epoxy		1.14	2.55	1.14	1.000

We focused our investigation on 2D GRIN PCs that were composed of different cylinder materials along different rows. The GRIN PC we used contained 19 rows of solid cylinders ($y=[-9a,+9a]$) arranged in a square lattice and embedded in epoxy, with a filling fraction of 0.126. The elastic properties of the cylinders and the epoxy are listed in Table I. The band diagrams of each row for the first SV-mode BAW are plotted in Fig. 3(a). The lowest initial frequency of the first partial band gap among all rows was $\Omega=0.31$, suggesting that the GRIN PC can operate over a wide band from $\Omega=0.0-0.31$. For frequencies below $\Omega=0.25$, the equal-frequency contours of all rows were nearly perfect circles of anisotropic ratios ($r_a=v_{\Gamma X}/v_{\Gamma M}$) less than 1.025. These ratios suggest that each row can be approximated as an isotropic medium. The effective refractive indices obtained at reduced frequency $\Omega=0.10$, per Eq. (5), are listed in Table I and plotted in Fig. 3(b) along with a best fit to the hyperbolic secant profile (solid black line). The effective refractive index of each row was a function of frequency because PCs disperse with frequency. Fitted profiles for different reduced frequencies [Fig. 3(b)] show that the gradient coefficient of the GRIN PC is dependent upon reduced frequency. Per Eq. (4), one can calculate the theoretical focal lengths at different reduced frequencies. We compared these theoretically calculated focal lengths to those from the simulated results, as shown in Sec. III.

III. SIMULATION RESULTS AND DISCUSSION

To investigate the capability of a GRIN PC in manipulating acoustic waves, we simulated the propagation of SV-mode BAWs by a FDTD method.[13,28] The FDTD program was developed per the theory of elasticity: the equation of motion and the constitutive law were discretized to simulate wave propagation in linear elastic materials. The simulation domain used for FDTD was a 2D GRIN PC that comprised 19 rows in the y direction and 50 layers in the x direction. The material properties of cylinders and the background are in Table I, the same as those used in the PWE calculation (Sec. II). An infinitely long line source was placed at $x=0$ and was defined by setting the initial body force in the equation of motion. The line source was polarized along the z

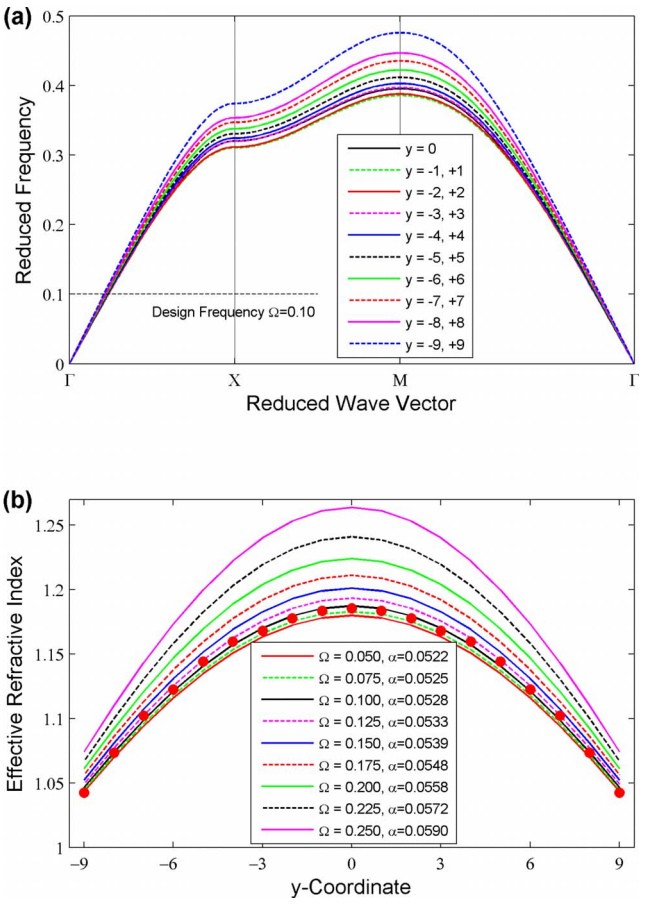

FIG. 3. (Color online) (a) The band diagrams of each row of the GRIN PC for the first SV bulk acoustic mode. The material properties are listed in Table I. (b) The fitted hyperbolic secant profiles for different reduced frequencies. The red dots represent the effective refractive indices at a frequency of $\Omega=0.10$. The gradient coefficient was found to be sensitive to frequency.

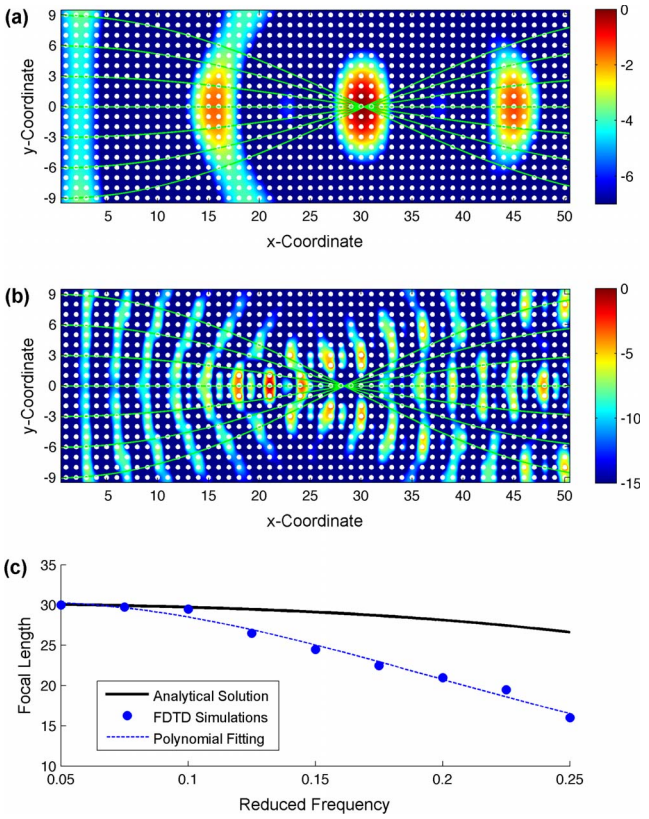

FIG. 4. (Color online) The FDTD simulated acoustic wave propagation in the GRIN PC at a reduced frequency of (a) $\Omega=0.05$ and (b) $\Omega=0.20$. The overlapped beam trajectories were calculated from Eq. (2). The amplitudes of displacement fields were normalized and presented in decibel scale. The x and y coordinates were in unit of a. (c) The calculated (solid line) and simulated (dotted line) focal lengths of the GRIN PC vs the operation frequency.

axis to generate a SV-mode BAW. The entire domain was surrounded by perfectly matching layers[29] at the boundaries to avoid numerical reflections in the simulation domain, resulting in total absorbance at the boundary. The lattice spacing a was set as 8 mm and each lattice was discretized into 20 uniform spatial grids. The other parameters used in the FDTD simulations were the same as those in the PWE calculations of Sec. II.

Figure 4(a) shows the simulated acoustic wave propagation at reduced frequency $\Omega=0.05$ along with the beam trajectory calculated from analytic expression in Sec. II. The amplitudes of displacement fields are shown in decibels (dB). The color distribution was normalized per the maximum value of the displacement. The figure shows the redirection of plane waves as they propagated within the GRIN PC and focused at $x=30$. This redirection matches with the theoretical value given by $f=\pi/(2\cdot 0.0522)=30.09$. The acoustic beams incident upon various y positions had different propagation routes toward the focal spot, but their propagation in the x direction was constant because the velocity of sound is inversely proportional to effective refractive index. As such, there is a token degree of longitudinal aberration within a GRIN PC. The focal spot has a −3 dB width (in the y direction) of $7a$, equivalent to 35% of the wavelength of SV wave in epoxy at $\Omega=0.05$ ($\lambda=a/\Omega=20a$), indicating minor transverse aberration. Figure 4(b) shows the propagation of acoustic waves at $\Omega=0.20$. The structure gradually deformed the planar wave fronts into circular wave fronts, focusing the acoustic beams at $x=21$ and collimating waves that would have otherwise diverged beyond that point. The −3 dB width of the focal spot was 55% of the wavelength. Figures 4(a) and 4(b) illustrate effective acoustic focusing over a wide range of $\Omega=0.05-0.20$ ($\Delta\Omega=0.15$), several times wider than the working band of a negative-refraction-based PC ($\Delta\Omega\leq 0.04$).[17–20]

The focal length of the GRIN PC versus the operation frequency is presented in Fig. 4(c). The solid and dotted lines represent the focal length calculated from gradient coefficients and obtained from FDTD simulations, respectively. The analytic solutions were close to the simulation results at reduced frequencies below $\Omega=0.10$. As the reduced frequency increased, the analytic results deviated from the simulated results. This deviation is most likely caused by the fact that at higher frequencies, the wavelength was comparable to lattice spacing. At small wavelengths one cannot assume that the gradient of the GRIN PC is smooth. The fact that EFCs are less circular at higher frequencies much or less contributes to the deviation. As a result, the analytic beam trajectory is only valid when the SV-mode wavelength in epoxy is at least ten times larger than the lattice spacing of the GRIN PC.

The simulated acoustic propagation in GRIN PC at $\Omega=0.10$ is shown in Fig. 5(a), as well as the beam trajectory calculated from Eq. (2). The displacement across the y section of the focal spot at $x=29.5$ was compared with that of an unfocused acoustic beam centered at $x=2.5$, as shown in Fig. 5(b). We also plotted in this figure the displacements of acoustic waves at $x=29.5$ in a domain filled with epoxy and in two PCs of cadmium/epoxy and niobium/epoxy. All curves were normalized to the maximum value of displacement at the focal spot of the GRIN PC. The amplitude drop caused by solid cylinders in regular PCs and the GRIN PC was about 40% of the displacement amplitude in epoxy; this coincides with the reflection coefficient calculated from effective acoustic impedances. The focusing capability of the GRIN PC is evident from the magnification and distribution of the displacement field along the y axis [black line in Fig. 5(b)].

Figure 5(c) shows the simulated displacement field of acoustic wave propagation in a domain filled with epoxy and a 20-layer-thick GRIN PC at reduced frequency $\Omega=0.10$. The planar acoustic waves were redirected within the GRIN PC and were focused outside the structure at $x=29$. These results indicate that GRIN PCs can serve as flat lenses that focus acoustic waves outside the structure. The focal spot was slightly longer and wider than that in Fig. 5(a) due to insufficient converging length. Nevertheless, we realized a clear shape of focal spot with −3 dB width of 60% of the wavelength.

The beam trajectories [Figs. 4(a), 4(b), 5(a), and 5(c)] which overlapped on the simulated displacement field were calculated from the analytic expression in Sec. II. For trajectories outside the GRIN PC, the slopes of these straight rays

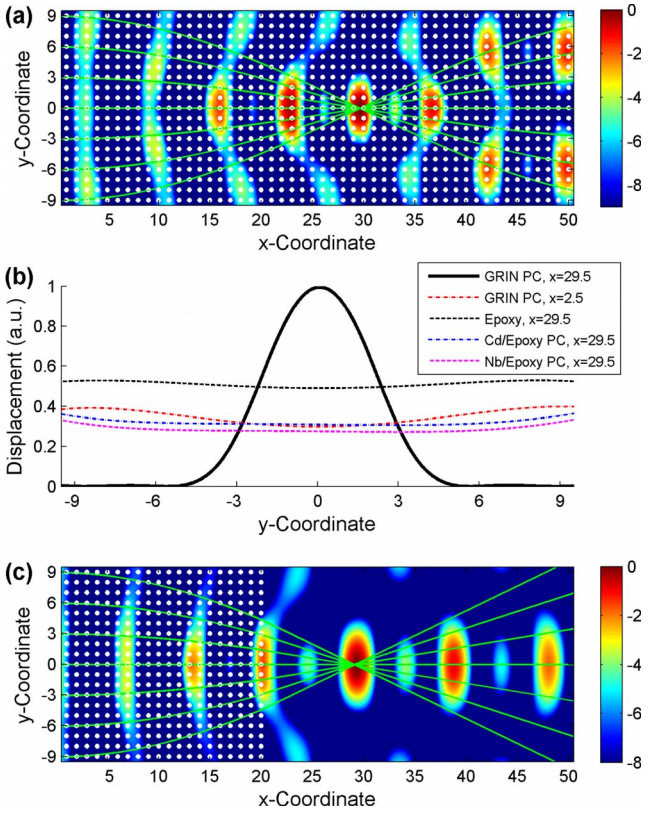

FIG. 5. (Color online) (a) The simulated acoustic wave propagation in the GRIN PC at a reduced frequency of $\Omega=0.10$. (b) A comparison of displacement fields along y section of the GRIN PC, epoxy, and two regular PCs. All curves were normalized to the maximum displacement at the focal spot of the GRIN PC. (c) The simulated acoustic focusing in a domain filled with epoxy and a 20-layer-thick GRIN PC lens at a reduced frequency of $\Omega=0.10$.

were calculated by taking the derivative of Eq. (2) at the interface ($x=20$) and considering Snell's law of refraction. The focal spot predicted by the ray-tracing calculation matches well with the FDTD simulation, as indicated in Figs. 4(a), 5(a), and 5(c). We concluded that the analytic expression can serve as a powerful tool in designing flat GRIN PC lenses for acoustic focusing when the wavelength in the background material is much larger than the lattice spacing of the GRIN PC. Compared to existing negative-refraction-based PC lenses, our GRIN PC lens possesses several advantages. First, the GRIN PC lens can operate over a wide frequency band below the first partial band gap, while negative-refraction-based PC lenses usually operate within a small range of partial band gaps. Second, a GRIN PC lens can be coupled with acoustic transducers and can effectively redirect paraxial incident acoustic waves to a small focal spot—the position of this spot is determined by the adjustable gradient coefficient. In contrast, with negative-refraction-based PC lenses one must focus select diverging waves to a long focal zone.[17] Finally, a GRIN PC lens can work at a reduced frequency range below $\Omega=0.10$, so it can be made much smaller than a negative-refraction-based PC lens and can be seamlessly integrated with existing millimeter scale acoustic systems.

IV. SUMMARY

GRIN PCs have been proposed to manipulate the propagation of acoustic waves. We numerically demonstrated that a GRIN PC of a hyperbolic secant refractive index profile caused acoustic waves to converge over a wide range at low reduced frequencies ($\Omega=0.05-0.25$), a range five times broader than those offered by existing negative-refraction-based PCs. The analytically calculated beam trajectories match well with FDTD-simulated results. Being a compact, flat acoustic lens with a wide operational frequency range, the GRIN PC described in this work can be useful in applications such as acoustic imaging, drug delivery,[30] high intensity focused ultrasound,[31] cell sonoporation,[32] sonofluidics,[33] and NDE.[34]

ACKNOWLEDGMENTS

We thank Xiaole Mao, Thomas R. Walker, Shih-Ho Cheng, and Aitan Lawit for helpful discussion. We received support from the High Performance Computing Group at the Pennsylvania State University. This work was supported by National Science Foundation (Grants No. ECCS-0824183 and No. ECCS-0801922) and the Penn State Center for Nanoscale Science (MRSEC).

*Author to whom correspondence should be addressed. junhuang@psu.edu

[1] E. Yablonovitch, Phys. Rev. Lett. **58**, 2059 (1987).
[2] M. S. Kushwaha, P. Halevi, L. Dobrzynski, and B. Djafari-Rouhani, Phys. Rev. Lett. **71**, 2022 (1993).
[3] T.-T. Wu, Z.-G. Huang, and S. Lin, Phys. Rev. B **69**, 094301 (2004).
[4] G. Wang, J. Wen, Y. Liu, and X. Wen, Phys. Rev. B **69**, 184302 (2004).
[5] V. Laude, M. Wilm, S. Benchabane, and A. Khelif, Phys. Rev. E **71**, 036607 (2005).
[6] J.-C. Hsu and T.-T. Wu, IEEE Trans. Ultrason. Ferroelectr. Freq. Control **53**, 1169 (2006).
[7] J.-C. Hsu and T.-T. Wu, Phys. Rev. B **74**, 144303 (2006).
[8] Z. Z. Yan and Y. S. Wang, Phys. Rev. B **74**, 224303 (2006).
[9] R. Sainidou, B. Djafari-Rouhani, and J. O. Vasseur, Phys. Rev. B **77**, 094304 (2008).
[10] J. Gao, X. Y. Zou, J. C. Cheng, and B. Li, Appl. Phys. Lett. **92**, 023510 (2008).
[11] J. Shi, S.-C. S. Lin, and T. J. Huang, Appl. Phys. Lett. **92**, 111901 (2008).
[12] A. Khelif, B. Djafari-Rouhani, J. O. Vasseur, and P. A. Deymier, Phys. Rev. B **68**, 024302 (2003).
[13] J.-H. Sun and T.-T. Wu, Phys. Rev. B **74**, 174305 (2006).
[14] Y. Tanaka, T. Yano, and S. I. Tamura, Wave Motion **44**, 501 (2007).

[15] Y. W. Yao, Z. L. Hou, and Y. Y. Liu, Chin. Phys. Lett. **24**, 468 (2007).
[16] J.-H. Sun and T.-T. Wu, Phys. Rev. B **71**, 174303 (2005).
[17] S. Yang, J. H. Page, Z. Liu, M. L. Cowan, C. T. Chan, and P. Sheng, Phys. Rev. Lett. **93**, 024301 (2004).
[18] K. Imamura and S. Tamura, Phys. Rev. B **70**, 174308 (2004).
[19] X. Zhang and Z. Liu, Appl. Phys. Lett. **85**, 341 (2004).
[20] L. Feng, X.-P. Liu, Y.-B. Chen, Z.-P. Huang, Y.-W. Mao, Y.-F. Chen, J. Zi, and Y.-Y. Zhu, Phys. Rev. B **72**, 033108 (2005).
[21] A. Hakansson, F. Cervera, and J. Sanchez-Dehesa, Appl. Phys. Lett. **86**, 054102 (2005).
[22] C. Gómez-Reino, M. V. Perez, and C. Bao, *Gradient-index Optics: Fundamentals and Applications* (Springer, Berlin, 2002).
[23] E. Centeno, D. Cassagne, and J.-P. Albert, Phys. Rev. B **73**, 235119 (2006).
[24] H. Kurt and D. S. Citrin, Opt. Express **15**, 1240 (2007).
[25] E. Akmansoy, E. Centeno, K. Vynck, D. Cassagne, and J.-M. Lourtioz, Appl. Phys. Lett. **92**, 133501 (2008).
[26] B. K. Juluri, S.-C. S. Lin, T. R. Walker, L. Jensen, and T. J. Huang, Opt. Express **17**, 2997 (2009).
[27] M. Ke, Z. Liu, C. Qiu, W. Wang, J. Shi, W. Wen, and P. Sheng, Phys. Rev. B **72**, 064306 (2005).
[28] P.-F. Hsieh, T.-T. Wu, and J.-H. Sun, IEEE Trans. Ultrason. Ferroelectr. Freq. Control **53**, 148 (2006).
[29] J. P. Berenger, J. Comput. Phys. **114**, 185 (1994).
[30] S. Mitragotri, D. Blankschtein, and R. Langer, Science **269**, 850 (1995).
[31] V. Zderic, A. A. Braymanb, S. R. Sharare, L. A. Cruma, and S. Vaezy, Ultrasonics **45**, 113 (2006).
[32] P. Marmottant and S. Hilgenfeldt, Nature (London) **423**, 153 (2003).
[33] J. Shi, X. Mao, D. Ahmed, A. Colletti, and T. J. Huang, Lab Chip **8**, 221 (2008).
[34] B. Tittmann, J. Du, and I. Lucas, Proc. SPIE **5770**, 114 (2005).